Insights on Physics of Hall Thrusters through Fast Current Interruptions and Discharge Transients.

Mathieu Prioul[*], André Bouchoule[*], Stéphanie Roche[**],
Lionel Magne[**], Daniel Pagnon[**], Michel Touzeau[**], Pascal Lasgorceix[***]
[*] GREMI, Université d'Orléans, BP 6744, 45 067 Orléans, France
[**] LPGP, Université Paris XI ORSAY, 91 405 Orsay, France
[***] Laboratoire Aérothermique, CNRS, 45 067 Orléans, France
contact: andre.bouchoule@univ-orleans.fr

IEPC-01-059

Spontaneous fluctuations or oscillations, with characteristic time scales of few tens µs are well known as one of the most evident instationary phenomena in closed electron drift thrusters (CEDT). They have been already characterised in many experimental studies and rather well reproduced by simulation studies. When looking at these spontaneous phenomena, time and space resolved data on discharge plasma and plume revealed interesting insights on the dynamics of these instabilities. As in various physical systems, the response to a controlled transient perturbation of a "stationary" state would be helpful for an insight on basic properties of the system in this stationary state. Such approach was developed for CEDT's by using fast current interruptions and looking at the various physical transients induced in plasma and plume. Most of these studies were done on SPT100 type CEDT.
The design and test of the current switch able to perform "instantaneous" ON-OFF transitions and the time and/or space resolved diagnostics are key points for such approach and are described or refereed. Results show that such approach opens a convenient way for physical study of these thrusters. New insights have been obtained on collisional-radiative processes, electron transport phenomena and connections between channel plasma and plume. Moreover, the development of wide frequency band diagnostics lead, for the first time to our knowledge, to a clear evidence of the connection between microinstabilities and macroscopic behaviour of the thruster current. These data emphasise the importance of refinements in modelling/simulation and seems to be useful for such progresses.

INTRODUCTION

From its beginning in the sixties (ref. [1], [2]), the achievement of the present performances of the CEDT's has been the result of both a basic physics insights on E×B plasma and of pragmatic structural improvements. The most important parameter, the magnetic topography, is the throughput of these crossed developments in terms of stability and performances. In spite of such a long-term research, simulations able to give confident designs of thrusters with fixed performances and long term reliability are not presently available. The reason is clearly the complex physics involved in such far from equilibrium plasmas, with strong spatial gradients and strong plasma-surface interaction phenomena. Electron transport phenomena, in the various regions from the external cathode to the anode at the channel bottom, remain up to now an open subject. For example parietal effects, as often involved in the channel, are involved in modelling studies through an adjustable collisional electron transport frequency. In spite of these open questions, the practical performances and reliability of these CEDT's systems lead to their strong interest for space propulsion and satellites technology. Thrusters SPT100 from FAKEL and PPS1350 from SNECMA for example will equip the technological satellite STENTOR. The fast increasing input of the CEDT's in this field reinforce also the requirement of a better basic knowledge able to help in advanced concepts and/or up-scaling projects.
The research program launched in France several years ago is devoted to this goal. In connection with

Presented as Paper IEPC-01-059at the 27th International Elecetric Propulsion Conference, Pasadena, CA, 15-19 October 2001.

CNES, SNECMA, ONERA, several academic research teams are involved for experimental (Aérothermique Orléans, GREMI Orléans, LPGP Orsay) and modelling/simulation studies (CPAT Toulouse, CPHT Ecole Polytechnique). The general frame of this program is described in another paper of IEPC 15 [3]. Results of this co-operative research have been reported in overview papers [4], [5] with an extensive bibliography.

One of the points developed in the previous studies was to obtain a detailed view on transient phenomena occurring during the spontaneous fluctuations of SPT100 discharge. Several new insights on these phenomena have been acquired by using time and space resolved diagnostics of both channel plasma and plume. The most important ones are (ref. [6], [7], [8], [9], [10]):

- a rather small instantaneous energy spread of the ejected ions (20 eV) with time varying mean energy
- a spatial fluctuation of ionisation/acceleration zone
- a correlated time varying divergence of the plume

These data were obtained by looking at the spontaneous fluctuating or oscillating regime of thrusters. The main aim of the present paper is to present the data obtained by using an external perturbation of the thruster regime. There are two key points in such approach. The first one is that repetitive, well defined in time, diagnostics are welcome for such instationary studies. The second one is that, as long as the time scale of imposed transients of the discharge is short enough, new data connected to "instantaneous" perturbations are available.

The first step to develop this research was to achieve such fast transients, to the thruster regime. Previous studies devoted to modelling the AC behaviour of SPT100 showed that the SPT discharge is almost a pure current equivalent source [11]. Moreover it is well known that DC behaviour is such that a current saturation is obtained at the nominal operating point. It means that the required fast transient is to be achieved by a current control device. The typical transient has to be significantly shorter than the natural response time revealed by spontaneous fluctuations, and then shorter than 1 µs.

The optically controlled switch able to satisfy such requirement is described in the first part of the paper, together with the time resolved diagnostics developed to obtain data on thruster, plasma and plume transient behaviour.

The transient OES data lead to new insights on collisionnal-radiative processes in the channel. They will be presented in Part II.

Several data concerning electron transport phenomena have been deduced from analysis of space-time dynamics of ionisation in magnetised domain of the channel. They are reported in Part III, together with the evidence of time localised bursts of microinstabilities related to spontaneous discharge current waveform. This last result is a new input on the possible role of such microinstabilities on electron transport in the channel.

PART I: Fast thruster current interruptions and related diagnostics

The experiments have been performed on the laboratory SPT100 ML thruster when running at nominal operating conditions: discharge potential of 300 V, anode xenon mass flow rate of 5 $mg.s^{-1}$ and discharge current of 4.2-4.5 A. This thruster was installed in the French PIVOINE facility [12]. In this 4 x 2 m cylindrical stainless steal tank, the cryogenic pumping system allows a working pressure of 2×10^{-5} mbar for a xenon mass flow rate of 5 $mg.s^{-1}$.

I 1: Fast switch of thruster current

A power MOSFET device able to perform very fast (0.15 µs) current interruptions and plasma extinction has been designed. A computer controlled pulse generator (Tti TGA 1230) drives optically the device in order to let the thruster to a floating potential (Figure 1). The duration of interruptions T_{OFF} can vary between 1 µs and 10µs, and repetition rate can be fixed in the range of 1kHz to 50kHz. The current extinction by such a device has been tested on a simulation resistive charge (300V, 10A), showing that its characteristic extinction time is less than two hundred nanoseconds as shown on the Figure 2. These characteristics have been confirmed for current interruption on the thruster electric feeding lines as shown on Figure 3.

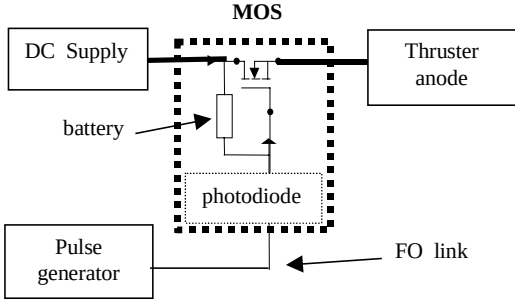

Figure 1: the discharge shutter

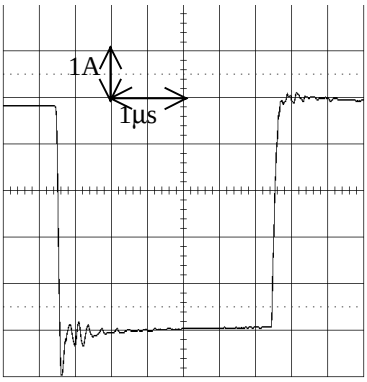

Figure 2: Discharge shutter test on a resistive charge.

The shutter is inserted on the electrical anode feeding line. Current is measured on the anode and cathode lines using 60MHz bandwidth Tektronix current probes (P6021). At low repetition rate (typically 1kHz), the discharge stationary state is restored before each switch operation: a highly repetitive behavior is observed (Figure 3) for a single or low frequency (1 kHz) repetitive interruption, when the thruster is in the spontaneous fluctuating regime of interest in this study. This behavior is characterized by:

- A phase of current extinction and optical emission relaxation during T_{OFF} (1. on Figure 3),
- A transient current peak just when the discharge is switch ON (2. on Figure 3),
- Low frequency (25 kHz), high amplitude relaxing oscillation (3. on Figure 3).

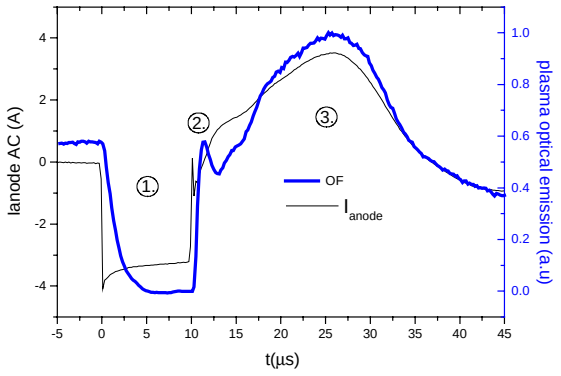

Figure 3: Discharge current and optical emission in the channel response to a current interruption.

I 2: In situ space and time resolved diagnostics of plasma and plume emissions

Several optical diagnostics have been used to study the plasma both in the channel and in the plume. An array of 16 UV optical fibers (OFA) has been designed to investigate the plasma in the channel through a thin slit in the external ceramic. These fibers integrate radially the plasma optical emission. Collimators are used to obtain an axial precision of 0.5 mm while space between fibers leads to an axial resolution varying from 0.5 mm in the ionization zone to 2 mm in the near anode zone. Figure 4 shows the installation of this OFA on the thruster structure.

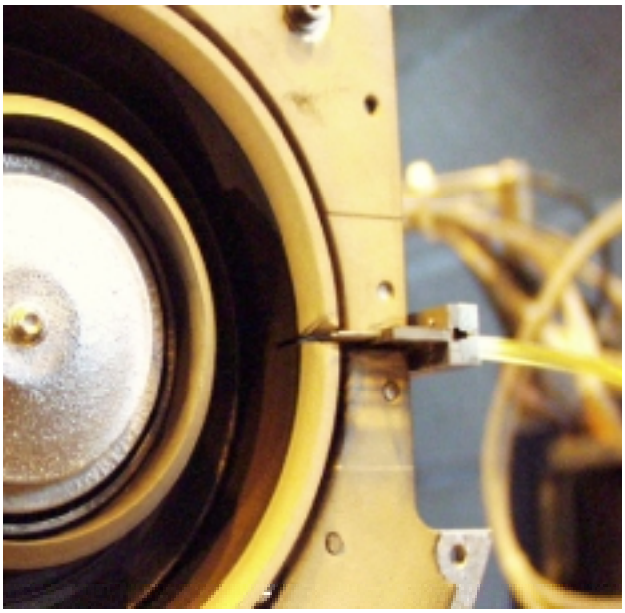
Figure 4: installation of this OFA on the thruster structure

The OFA has been initially calibrated using a thin light source moved in front of each collimator. During the campaign of measurements, the axial time averaged emission profile has been regularly updated to take into account possible modification due to collimators erosion. Depending on its use it can provide time and/or space and/or wavelength resolved measurements in the channel:

- All fibers can be connected to a 16-channel photomultiplier and data acquisition system equipped with spectral band pass filters selecting ionic or neutral emissions. It allows the simultaneous recording of the 16 signals at 160 kHz sampling rate or the recording of fast transients with a good noise-signal ratio on a 4 channel 500MHz scope.
- Each fiber can be connected to the entrance slit of a 64 cm monochromator (HRS-640 Jobin-Yvon) equipped with a photon counting photomultiplier (PM). This 10ns single pulse PM is connected to a multi-scale analyzer (SR430: amplifier/discriminator and pulse counter) synchronized on the current interruptions. Accumulations over 100 000 pulses, 4000 depth, 40 ns width gates allow to

obtain 160 µs length, 40 ns time resolved light signals emitted by neutral and ionic xenon excited states.

I 3: Electron drift current diagnostic.

A wide band inductive probe has been used to measure the azimuthal electron drift current. This loop, inserted in a trench performed in the external ceramic is connected to the R = 50 Ω input of a 600 MHz sampling rate Tektronix oscilloscope through a 50 Ω vacuum seal. The recorded signal e(t) is related to magnetic flux variations Φ(t) viewed by the loop through the usual relation:

$$\frac{d\Phi}{dt} = L\frac{di}{dt} + e \quad where\ e(t)\ is\ R\,i(t)$$
$$or \qquad j\omega\ \Phi_{\omega} = (jL\omega + R)\ I_{\omega} \quad for\ harmonic\ signals$$

Indeed, in the frequency range of interest here, this electrical system is a quasi-stationary one: dimensions are negligible in comparison with the signals propagation wavelength.

This inductive probe has been calibrated by using a harmonic (or pulsed) current loop I_{exc} simulating the electron drift current as source of the magnetic flux Φ (t). This was achieved by a using a copper loop, with a diameter equal to the mean thruster channel one and located near the channel output plane. For AC calibrations a power amplifier is used to launch simulation currents in the frequency range 1-50 kHz and amplitude 10-40 A peak-peak. The experimental harmonic gain defined by $e_{\omega} = f(I_{exc\omega})$ is shown on Figure 5 (amplitude in mV/A x kHz, phase in degrees).

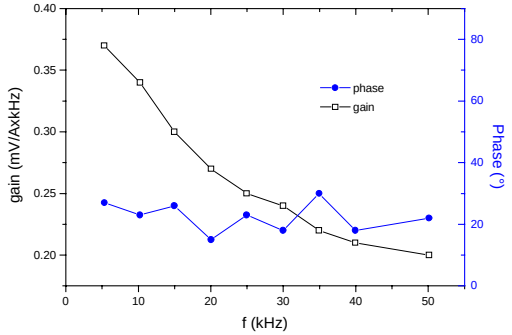

Figure 5: Experimental harmonic gain and phase.

As can be seen the transfer function I(t) → e(t) is close to the behaviour of pure integrator. This was expected from the previous relation, taking into account the very low value of the self-inductance of the detecting loop, leading to a negligible contribution for this frequency range in the transfer function.

This calibration has been made for various positions in the range of ± 5 mm around the exit channel plane. Data show that the transfer function gain is not sensitive to the exact position of the excitation loop. It means that signals recorded when e(t) is induced by variations of the electron drift current are representative, with a good approximation, of the variations of the electron azimuthal current intensity, even if this current moves in space.

This probe has been used for measurements of the electron drift current in the spontaneous fluctuating regime of the SPT 100. The Figure 6 shows the data obtained for I_{fd} and for $I_{fH,}$ discharge and electron drift current variations.

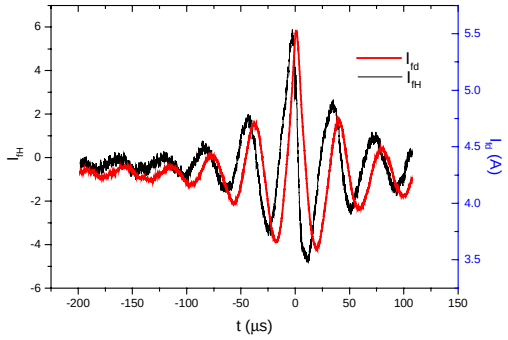

Figure 6: Dicharge and Hall current spontaneous evolution

The ratio I_{fH}/I_{fd} is close to 5. These data was obtained for a relatively low fluctuation level (20-30 %) in the thruster current. A simple assumption is that the same ratio apply for time averaged DC values of these currents. Such an assumption leads to DC electron drift current of 20 A for a DC discharge current of 4.2 A. This value will be confirmed below by using a pulsed regime for calibration and the fast switch for electron current extinction.

It can be noticed, as it is well known, that the electron drift current is related to the thrust of the system ([13], [14]). This force is the Laplace force between the electron current loop and the radial component of the coils magnetic field. Taking into account the length of this current loop (27 cm) and the nominal thrust (80 mN) the radial magnetic field is derived, with a value of $1{,}55.10^{-2}$ T. This averaged magnetic field is very close to the real value of the radial component of the magnetic field, near the channel output and at the channel mean diameter.

If the Hall current is assumed to be radially uniform it is possible to derive an order of magnitude of its longitudinal extension by using data obtained by LIF measurements [15] and numerical simulations

[16]. Both leads to longitudinal electric field of the order of 3.104 V/m in the acceleration zone and the electron density is predicted in the range of 10^{18} m^{-3}. These data lead to azimuthal electron velocity of $2\ 10^6$ m/s and to a longitudinal extension of the electron drift current of 5 mm. It is interesting to note that, besides its rough derivation here, this value is consistent with data given for example in ref. [14].

A different way to measure the DC value of the electron drift current is available by using the fast switch and measuring the transient loop signal related to the extinction of the plasma. Of course, the very high frequency band concerned by such fast transients requires a specific calibration. The same copper loop has been used to simulate fast interruption of the electron drift current loop, by installing the copper loop in the circuit described above (fast switch and resistive load). This test leads to a calibration factor $\eta = \Delta e/\Delta I_{exc}$ where Δe is the jump measured on the loop signal and ΔI_{exc} is the jump in the loop current. The value of η is measured as $\eta = 0.15$ V/A.

The discharge current $I_d(t)$ and loop signal e(t), recorded with a two channels fast sampling scope, are shown on Figure 7. Taking into account the calibration this leads to a Hall current jump of 23 A, in very good agreement with the estimation made by using data recorded in the spontaneous fluctuating regime.

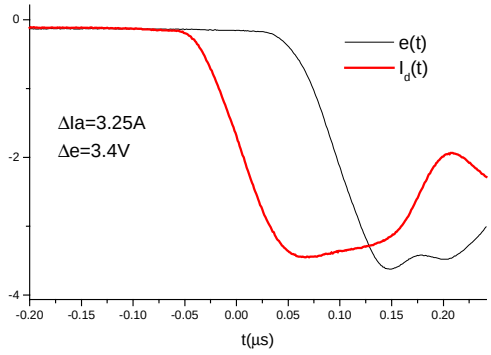

Figure 7: Discharge current and inductive loop signal when the discharge is switched off.

In fact this experiment is even more instructive. When looking at these signals we see that a very small delay is apparently observed between the current extinction and the electron drift current drop. In fact this delay, if any, is even smaller, due to the length of the cables involved in the signal transmission from the loop to the scope (15 m or 45 ns). So the most interesting result is that the electron drift current drops to almost zero value in a very short time: 150 ns. As will be shown later it is clear that the electron density cannot decrease at such characteristic time. It means clearly that the longitudinal electric field, driven the electron drift current, is cancelled in this very short time. We will see later that this information is of prime importance for the analysis of the plasma relaxation when the thruster current falls down.

This result is consistent with a simple analysis: when the anode current is switched OFF, the current extinction is achieved at any place in the channel, which means a fast drop of both ionic and electronic currents. The longitudinal electron transport is induced by collisions with neutrals or sheaths and can be written as: $I_e = qn_e\mu_{e\,eff}\,E_z$ where $\mu_{e\,eff}$ is the effective electron longitudinal mobility. As already mentioned, the electron density can't vanish at the very short time scale of the current decay (150 ns) and the fast drop of the anode current imply also a fast drop of the longitudinal electric field in the channel. Electrons being frozen along magnetic field lines, the ions are no more accelerated and can't longer escape from the discharge channel, due to the space charge effects.

The conclusion is that, at the end of the anode current drop, electrons and ions cannot move axially and the plasma relaxation is connected to local volume processes or radial losses towards the ceramic surface of the channel. This relaxation will be discussed in details in Part II.

I 4: Optical diagnostics of transients in the plume

Two complementary diagnostics have been used to record optical emission transients.

The first one is by using a collimated optical fiber able to record photons emitted along its viewing direction, with a transverse resolution of the order of 1 mm. This fiber is located in front of an UV quartz window of PIVOINE facility and is viewing the plume transversally. It is mounted on a vertically and horizontally movable holder, controlled by computer. The fiber output is connected to the entrance slit of a monochromator. The wavelength-selected signal is acquired by using a photon counting technique triggered by the fast switch signal. These time resolved data are reconstructed at the end of the acquisition runs, leading to a spectral-space-time information.

This procedure is long and another one, faster, has been used to obtain time-resolved data on transient phenomena in the ion plume. A Princeton Instrument CCD camera with a gated pulsed intensifier, is viewing the thruster plasma with the

same 90° sight-view from the thruster axis. The plume images are obtained in a fast imaging mode, with a time resolution in the µs range, with a quartz long focal Nikon objective. Spectral filters have been used for selecting ions or neutral emissions but, as shown by spectroscopic analysis, most of the observed photons in the plume are related to ionic emissions. These time resolved images are used to derive the evolutions of the f(r,z,t) optical emission densities by using an Abel transformation procedure.

I 5: Analysis of the plume by time of flight effect.

Standard retarding potential analysers (RPA) are not able to select the contribution of xenon ions in their various charge states. A small size time of flight analyser has been designed in our laboratory. Data obtained with such device have been already published [17]. A simpler approach has been used here, using the previously described characteristics of the current interruption. With such a fast current and electric field drop there is also a very fast interruption of the ion flow launched by the thruster. The time of flight effects make possible to measure the various contributions to the drop in the ion flow signal at some distance of the thruster. This ion flow drop can be energy selected by using the collector signal of a RPA. By triggering the RPA acquisition on the thruster current switch the contributions to the ion flow of various charge state ions can be deduced from time of flight effects. Moreover the energy selection of the RPA allows measuring the energy distribution of these ions. Finally, as the RPA is fixed on a movable holder designed in such a way that it remains aligned with the thruster output line-sight, radial evolution of these various contributions can also be recorded over +/- 12° from the thruster axis.
An example of signals recorded without energy selection (repelling voltage of few tens Volts) is given Figure 8. The validity of those TOF measurements has verified by analysis of TOF data at various discharge potentials (Figure 9). Single charged ions are found to be created Δ = 30V under the discharge potential. Previous data have shown that ions have small energy dispersion [18] and the present ones show that the regions where various ions are created have not strongly different potentials.

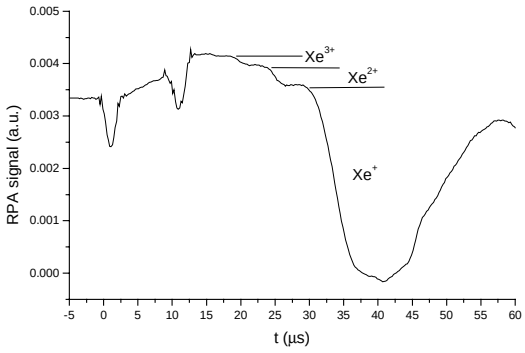

Figure 8: Typical TOF signal

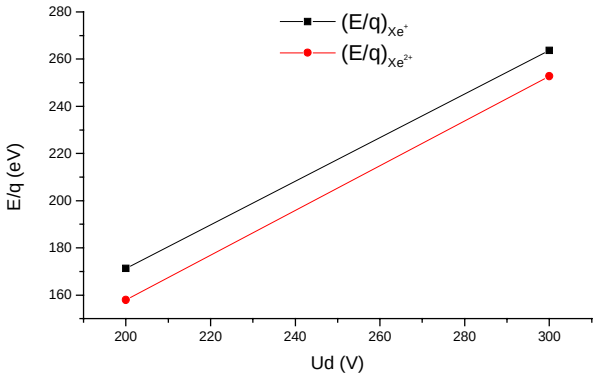

Figure 9: (energy/charge) ratio at various discharge potential

Some details on the various ion contributions in the plume and on relevant creation processes in the thruster are given below in part II.

PART II: Insights on collisional and radiative processes in channel plasma and plume

II.1: Data derived from current extinction and plasma relaxation.

II.1.2. Relaxation of high-energy electrons (T_{OFF}=10µs).

When quenching phenomena are negligible, as in the corona approximation, the radiative emission of an excited level j, populated from initial states *i*, is a direct information on the electronic excitation rate $n_i n_e \langle \sigma_{ij} v_e \rangle$. For most of the levels concerned here, with radiative life times of few 10 ns, this approximation is a rather good one in the thruster plasma. But stepwise processes involving metastable states can make invalid an other approximation of use in most simulations: the initial

state is restricted to the fundamental state of the species. Even in such case, if the variation of concentration of the bottom levels can be neglected in a very short time of interest where upper level emission variations are recorded, this open the way to obtain an information on the evolution of the electron population through the excitation rate.

This evolution is related to all collisional-radiative processes, energy losses by ionization and electron density decrease due to interaction with walls. This approach has been used in the post discharge period to obtain some insights on various loss terms of high-energy electrons, connected to inelastic collisions and losses towards the walls

The wavelength integrated plasma emission gives already an order of magnitude of the time scale of interest, through the evolution of $\Sigma_{i,} (n_i n_e <\sigma_{i,j} v_e>)$. This value, as shown on Figure 3, is τ_O = 1µs much longer than the current extinction time (Figure 3).

This τ_O value is clearly related to processes involved in the evolution of the high-energy electron concentration. Electrons and ions being axially frozen during the current interruption, it is possible to consider a 1D model to estimate electron density losses at the walls. Assuming at first order a Maxwellian distribution, and charge losses through the two sheaths surrounding the plasma defined by the Bohm flux: $\Phi_{Bohm} = 0.6\, n_e \sqrt{\frac{kT_e}{M_i}}$, the characteristic decay time of electron density is $\tau_{wall} = \frac{R_{ext} - R_{\min}}{2 \times 0.6 \sqrt{kT_e / M_i}}$, where R_{ext} and R_{min} are respectively external and internal channel radius. The evaluation of this time in the high magnetic field zone, where the electron energy is high, leads to an estimation of the minimum value of this time. For an averaged electron energy kT_e = 16 eV, it leads to $\tau = 3.5$ µs. In comparison, the characteristic decay time of electron energy by inelastic collisions can be derived from the ionisation frequency. Assuming a neutral density of 10^{19} m^{-3}, an ionisation cross section of σ_i =4.10^{-20} m^2 for the previous electron temperature, the mean time of electron energy loss is about 1 µs. This is in good qualitative agreement with τ_O whereas the characteristic decay time of electron density is longer. Therefore, on the τ_O time scale the electron population evolves mainly through energy cooling by destruction of the energetic part able to induce inelastic processes. This conclusion is confirmed, both for ions and neutrals emissions, by the strong correlation observed between the axial evolution of this characteristic time τ_{Oi}, τ_{On} and of optical emission intensities (Figure 10). Optical emission reveals also the frequency of these inelastic processes, in an electron energy range close to the ionisation threshold.

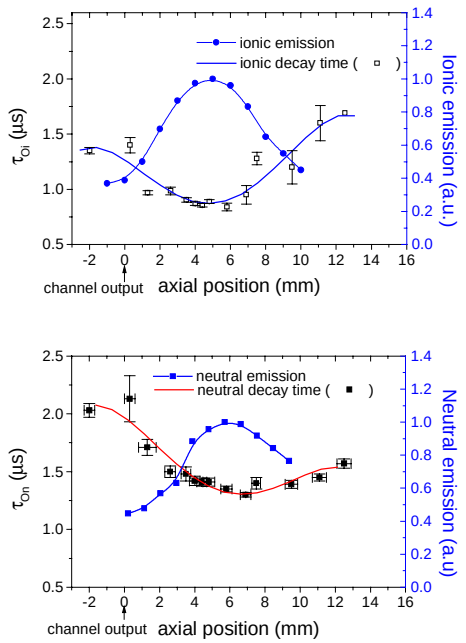

Figure 10: Evolution of the characteristic emission decay time compared to the stationary emission both for ions and neutrals.

This result shows that transient data obtained in short initial relaxation of the plasma are able to give insights on the stationary state before current interruption. The above data emphasise two other interesting features.

- The first one is that there is a noticeable difference in the spatial shape of ionic and neutral emissions. The ion excited states radiation is maximum in the domain of decrease of neutral emissions. It means that the ionic excited states are mostly obtained by involving electron-ion collisions and not electron-neutral collisions.
- The second one is that a significant difference is observed in the τ_0 values relative to ion and neutral excited states in the magnetised domain. This observation is consistent with the cooling by inelastic collisions for two reasons: the threshold for excitation is lower for neutrals and, especially in the domain of channel exit the neutral concentration is low and the corresponding collision frequency is lower. Inversely, closer to the anode, the ion density is lower and the inelastic collisional cooling is mostly defined by electron-neutral collisions and the relaxation of ion emissions becomes closer to the value measured for neutral emissions.

At the end of this decay of density of high energy electrons, the less energetic electron population relaxes mainly through losses towards the plasma surrounding surfaces, and mainly radially in the magnetised region of the channel. This relaxation is revealed by the behaviour of the anodic current, when the switch is turned ON at increasing values of T_{OFF} .

II.1.2. Relaxation of electron population for large values of current interruption

As shown in the Figure 11 a fast initial current peak appears when the discharge is switched ON. A similar transient optical emission peak occurs simultaneously at any place in the channel (Figure 3 and Figure 16). This initial burst in current and optical emissions is characterised by strong differences with the large amplitude signal appearing later with a smother time variation. The explanation, as detailed below, is that the fast peak is related to the reactivation of the electric field in the low plasma density channel while the following one is due to the propagation of an ionisation wave initiated by electrons coming from the channel output and moving towards the anode.

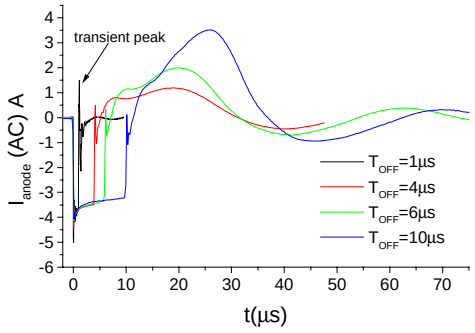

Figure 11: Evolution of the discharge current for different current interruption duration

The variation of the current peak intensity with T_{OFF} is shown on Figure 12. For T_{OFF} larger than 4 µs, the current peak intensity has a characteristic decrease time of 9 µs. A detailed model of density-energy relaxation of the electron population in this time domain, involving losses of electrons through the sheath surrounding the plasma, remains to be achieved. Nevertheless, this peak intensity behaviour is clearly connected with electron density relaxation during the T_{OFF} period. When using the loss model given by the Bohm flux, sensitive to the square root of electron energy, the characteristic decay time of 9 µs is consistent with electron energy of the order of 2.5 eV. It means that the loss of the high-energy electrons is mainly achieved at 4 µs values of T_{OFF}.

A detailed analysis of this initial relaxation (t<4µs) clearly involves a modelling taking into account the losses of high energy electrons and the creation of low energy electrons by inelastic processes and by energy selected escape from the plasma. Such a model has not been yet developed but the above considerations show that this approach using transient data appear as a powerful one for giving insights on inelastic processes and electron energy in the stationary regime.

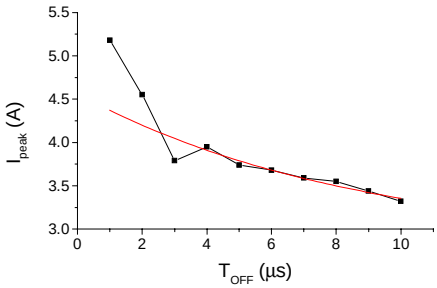

Figure 12: Evolution of the transient peak intensity with T_{OFF}.

Instantaneous emissions appear simultaneously along the channel as shown on Figure 16, when the switch is turned on. It means that the few cold electrons remaining in the channel at 10 µs are reaching energies in the range of 14 eV simultaneously. This suggests that the instantaneous electric field distribution is restored much more homogeneously than in the stationary state. The relative intensity of the emission peak is observed to be stronger in the near anode region. This is also consistent with the above interpretation, as the energy acquired by electrons is not limited by the magnetisation in this area.

An other interesting observation is the fast transient concerning the relative intensity of the spectral lines referred in table 1. The emissions for which the metastable states are involved in the upper level population appear less intense than expected from data in the stationary state. It means that the metastable concentration is lower than in the stationary conditions and that plasma equilibrium is not achieved on this short time scale shorter than 1 µs.

II 2: evidence of stepwise excitation processes in the channel plasma

II.2.1. Spectral emissions

lines	Emitting level	Excited from	energy	τ_{output}	$\tau_{8\ mm}$
XeI 823.2 nm	$2p^6$	1s5	1.51 eV	2.7 µs	1.7 µs
XeII 529.2 nm	$6p^4P^0_{5/2}$	$5d^4D_{7/2}$	2.06 eV	2.0 µs	1.2 µs
XeI 462.4 nm	$3p^6$	1s5	2.08 eV	2.1 µs	1.4 µs
XeII 484.4 nm	$6p^4D^0_{7/2}$	$5d^4D_{7/2}$	2.27eV	1.9 µs	1.2 µs
XeI 828.0 nm	2p5	XeI fund.	9.93 eV	1.2 µs	0.7 µs
XeII 460.3 nm	$6p^4D^0_{3/2}$	XeII fund.	14.48 eV	1.1 µs	0.7 µs

Table 1: Characteristic decay time for different lines.

The characteristic decay time of a given spectral line gives an insight on the evolution of the density of the electrons involved in the population of the upper level of the transition. Various energy thresholds are involved, depending on the upper energy level and on the lower one involved in the collisional process. The decay times for atomic and ionic lines have been recorded by using the photon counting technique. Data obtained for 6 spectral lines and for two positions along the channel are reported on table 1. These data evidence significant differences, leading to some insight on atomic physics involved in the plasma.

The possible contribution of electron collisions with metastable states in the population of upper states is indicated on the table by specifying the level involved. It is clear that a strong correlation exists between such low energy processes and the measured relaxation times of emissions. The destruction time of neutral metastable states by collision to channel walls, taking into account data on gas temperature (500 °C, ref. [4]) is negligible on the time scale of interest here. The same remark can be applied for metastable ions, as shown in part I.

Such detailed data show that these selected emissions can be divided in two groups:

- Lines with a characteristic decay time roughly equal to 1 µs: XeI-828.0 nm and XeII-46O.3 nm.
- Lines with a characteristic decay time roughly equal to 2 µs:XeI-462.4 nm, XeI-823.2 nm, XeII-529.2 nm and XeII-484.4 nm.

Similar characteristic decay times are observed for XeII-460.3 nm and XeI-828.0 nm lines. Electron energies involved in the population process are in the same energy range (9.93-14.48 eV), much lower than the energy required for the creation of the excited ion level from Xe neutral ground state (26.61 eV).

For XeI-462.4 nm and XeI-823.2 nm the characteristic decay time (2 µs) is significantly higher. It means that the relevant $2p^6$ and $3p^6$ levels are excited by lower energy electrons than $2p^5$ level.

The main conclusion is that the excitation of $2p^6$ and $3p^6$ levels involve significantly the metastable relay 1s5, while $2p^5$ level seems to be mainly populated from ground state.

The same argument can be applied to the decays of ionic states $6p^4D^0_{3/2}$, $6p^4P^0_{5/2}$ and $6p^4D^0_{7/2}$: the first one decreases faster. Excitation of $6p^4P^0_{5/2}$ and $6p^4D^0_{7/2}$ electronic inelastic collisions from the metastable relay $5d^4D_{7/2}$ seems to be efficient at least during the post-discharge.

The above data are related to specific lines and upper levels, while the previous ones (Figure 10) were concerning ion and neutral emissions viewed through broadband spectral filters. These data on specific lines reveal details of atomic physics processes and are of interest for spectroscopic diagnostics and for modelling. Further work in this direction will be useful to obtain data on the influence of metastable states in excitation/ionisation processes. Such data should help in improving the atomic physics schemes at work in simulations.

Analysis of plume emissions recorded in the stationary thruster regime reinforce these state selective behaviours; they are detailed below

II.2.1. Plume emission.

The Figure 13 represents the stationary spatial distribution of emission rates of the two ion lines referred above, measured in the SPT 100 plume. Like for their transient behaviour discussed above, these distributions show significant differences. The most evident one is that the excitation of the 529.2 nm line is much more pronounced in the

region, far from the exit, where the electron energy has been measured in the range of 3-5 eV.
In this domain the most probable excitation process is a low energy one. The relative higher intensity observed along the axis in the focusing region of the plume is consistent with the above conclusion: metastable ions should be implied in the population of the upper level of this transition. The ion density in this zone is rather high and can be deduced from the local ion beam velocity and current density. These values are respectively of the order of 20.000 m/s from LIF data [15] and 40 mA/cm^2 (ref. [19]). The neutralising electrons have the same concentration, estimated to be at least 1.5 10^{11} cm$^{-3.}$
The quenching cross-section for electron-xenon metastable ions is not available. There are some determinations of quenching argon metastable ions by electron (T_e = 1 eV). The corresponding cross-section is σ_{QAr} = 4.5 10^{-20} m^2 (ref. [20]). The cross-section for electron-xenon metastable ions is at least of the same order of magnitude. The velocity of ions is 20.000 m/s and the value of the residence time τ_r $\cong 10^{-6}$ s in the focussing region of the plume can be deduced from the emission map (Figure 13:). An electron mean energy of 3 eV in the region of interest can be assumed to estimate the probability Π_Q of xenon metastable ions to be quenched in the interaction volume: $\Pi_Q = 1-\exp(-\nu_Q\tau_r)$, where $\nu_Q = \langle n_e\sigma v_e\rangle$. This leads to the value $\Pi_Q = 1$. The relative concentration of metastables in the ion beam is not known. Nevertheless, the experimental observation if this quenching is consistent with a relative concentration as low as 1%.

II 3: energy and angular data for X_e^{n+} ions in the plume in the stationary state.

As explained in part I, time of flight effects can be used, in the fast current interruption regime, to record the contributions of various Xe^{n+} ions in the local ion current. These contributions have been characterised in terms of energy distribution. The Figure 14 shows results of this analysis for single and double charge ions. These energies are defined as total energy divided by the charge and represent the potential where are created these species. The broadening induced by the transfer function of the analyser is 18 eV and the width of these distributions is of the order of 30 eV, in agreement with previous data [18].

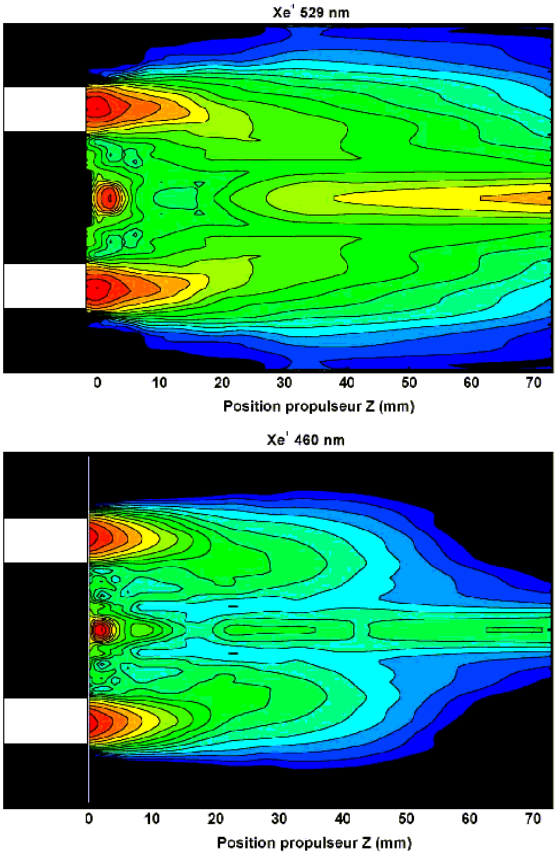

Figure 13: Xe^+ 529.2 nm and Xe^+ 460.3nm spectral line evolution in the plume.

The reduced mean energies are measured as 275 eV and 250 eV for single and double charged ions. It means that the second charge is acquired in mean in the plasma zone where the plasma potential is 50 volts lower than the first ionisation. Previous LIF data lead to the electric potential distribution obtained on the same thruster [15]. They show that the second ionisation is achieved at a close distance (<4 mm) from the ionisation zone. It means that the Xe^{2+} source is clearly localised in the channel, near the channel output.
An other conclusion is that the single charge ions involved in this second ionisation process have an average velocity of 8.000 m/s, corresponding to the 50 eV difference in the first and second ionisation processes. Their residence time in a layer of 3-4 mm of the drifting electron cloud is of the order of 0.5 µs. If we assume that 10% of ions are doubly ionised we can infer that this second ionisation is characterised by a typical ionisation time of 5 µs. This value is related to the local concentration of electrons of energy higher than the threshold energy (E = 21.2 eV) if the ionisation process involves single charge ions in their fundamental state. For an ionisation cross section $\sigma_{+->++}$ of 10^{-20} m^2 (ref. [21].) the above characteristic time needs a density

$n_{eH} > 5\ 10^{12}$ cm $^{-3}$ for electrons having energies above this threshold. This is even more than the total concentration of electrons in this domain. This evaluation suggests that the double ionisation involves another process with higher cross section and/or lower energy threshold. The most relevant interpretation is that this second ionisation should be related to ionisation of metastable single charged ions. The large value of the LIF signals obtained in LIF measurements in the channel reinforces this interpretation, taking also into account that ionisation from metastable ions should have higher cross sections.

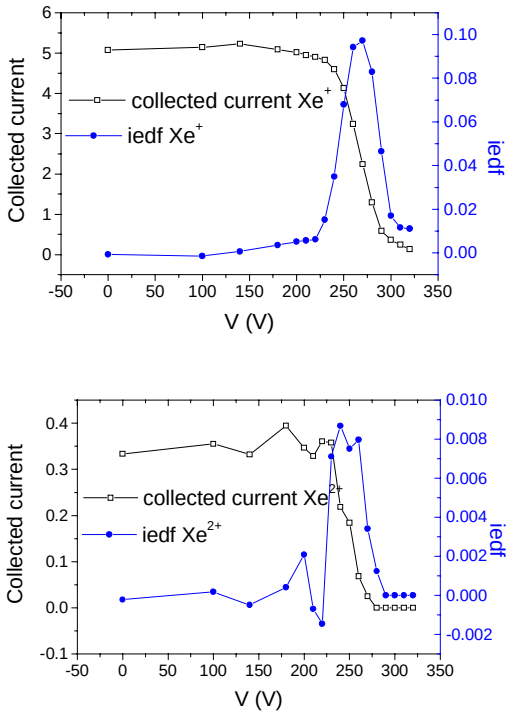

Figure 14: RPA collected current and iedf for Xe^+ and Xe^{2+} ions

The percentage of multiply charged ions in the plume is of interest not only for atomic physics considerations but has clearly consequences in terms of thruster performances. We saw that double charge ions are created at potentials significantly lower than single charge ions and this has a direct impact on thruster efficiency and averaged specific impulse. Such questions should be considered in modelling studies and the present data show that a more detailed atomic physics basis is probably required to reach such goal.

Another consequence of this space delayed secondary ionisation process is that the trajectories of these ions in the plume should be defocused in comparison with trajectories of single charged ones. The reason is that the electrical lens at work in the channel is defined at first approximation by the magnetic topography [1]. The single charge ions are created in the zone where they experience focusing effects in the ionisation zone while the added charge is achieved closer to the channel output and experience mainly defocusing effects. This is consistent with the measurements of the angular distribution of the two components obtained, as explained before, by recording the TOF signals at various radial positions. The data shown on the Figure 15 are in agreement with the above consideration. They emphasize two peculiarities: The first is that the contribution of multiple charge ions is a local parameter in the plume, with an increase when the direction is more out of axis. The second is that these data reinforce also the interest of 2D modellings able to take such phenomena into consideration.

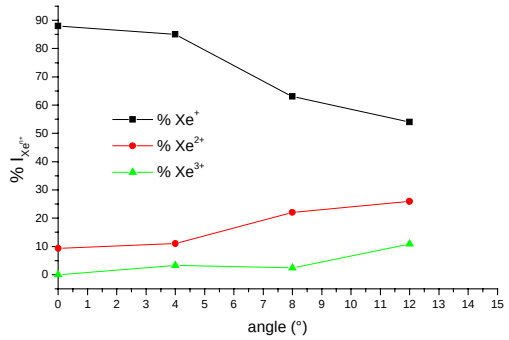

Figure 15: Angular charge state distribution.

PART III: Electron transport phenomena and dynamics of discharge and plume

III 1: Ionisation and plume dynamics at discharge re-ignition

The short initial transient of the discharge current is followed by a larger and longer current burst relaxing towards the stationary state, with a time behavior close to spontaneous oscillations. Normalized plasma emissions, recorded at various positions for T_{OFF} = 10 µs, are shown on Figure 16.

A clear space-time dynamics of this excitation ionization process is observed and is discussed quantitatively below in terms of electron transport. Qualitatively this behavior is the same as already reported for spontaneous fluctuations [11]: an ionization wave propagates from the outer part of the channel towards the anode and successive neutral depletion-refilling phenomena lead to the observed thruster current shape.

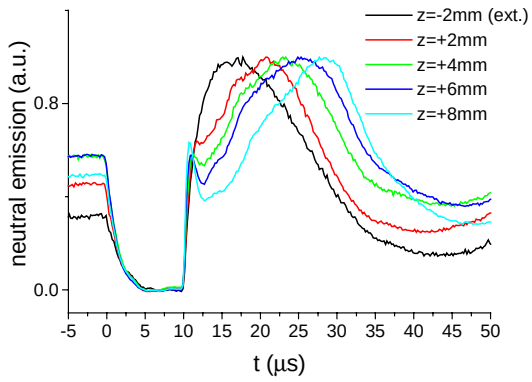

Figure 16: Normalised excitation-ionisation burst along the channel.

The displacement in time of the ionisation in the channel has significant consequences in terms of angular distribution of ejected ions, as shown on Figure 17 by some of the plume images obtained by the CCD camera.

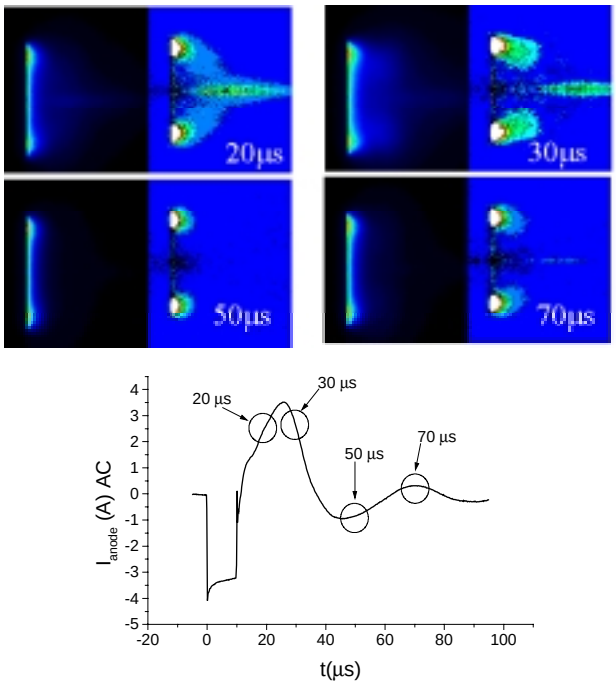

Figure 17: Time resolved behaviour of the plume.

On the thruster axis, the ion current density in the plume corresponds to ions outgoing from the full surface of the channel. For out of axis positions, only ions emitted from a restricted area can be collected. The location of this area is on diametrical plane defined by the considered point in the plume. These geometrical considerations explain why the thruster axis appears as a singularity. The position of the light emitted along this singularity, near axis, give information on the ion ejection angle. Figure 17 shows the evolution of the plume shape (obtained by fast CCD camera pictures and Abel transformation) at several characteristic periods of the current oscillations. It confirms the strong correlation between the localization of the ionization zone and the ejection angle of ions [11]. During the current increase ions are ejected with wide angular distribution while the ionization zone is localized nearer to the channel output. When the ionization zone moves upstream, in a region where the ionization rate falls, this lead to both a current decrease and a reduction of the ion ejection angular distribution. Ion focalization is carried out by the electrostatic lens, which is strongly correlated with the magnetic force lines at the channel exhaust. The ionization zone localization compared to the electrostatic lens position controls the ion ejection angle.

III 2: axial transport of electrons

III.2.1 Axial transport of electrons in the SPT100 ML thruster

The light signals observed by optical fibbers leads to the axial velocity of the excitation-ionisation wave involved in the first maximum of oscillation. The axial location of the first maximum of ion emissions is shown in Figure 18, as a function of axial position in the channel.

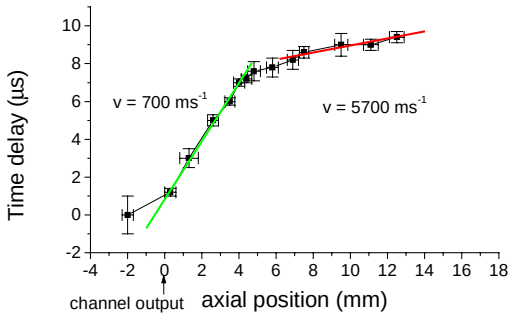

Figure 18: Evolution of the time of maximum emission along the channel.

A velocity of 700 ms^{-1} characterises this emission-ionisation burst propagating in the region of high radial magnetic field. This velocity can be compared to a classical electron drift across the magnetic field induced by elastic collisions with neutrals. This axial velocity v_z is given by $v_z = \nu r_c$ where ν is the average electron-neutral elastic collision frequency for electrons and r_c the local electron gyroradius given by $r_c = \frac{m_e E}{qB^2}$. A 170.10^{-4} T radial magnetic field [22] and a 2.10^4 $V.m^{-1}$ axial electric

field (from LIF data [15) lead to a gyroradius of 0.4 mm in the considered zone. Assuming that the electron transport is carried out only by electron-neutral elastic collisions, it would lead to an estimation of the average electron-neutral elastic collision frequency for electrons ν =1.75 × 10^6 s^{-1}. This frequency is derived from electron-neutral momentum transfer cross-section ($\sigma = 2\times10^{-19}$ m^2), the electron temperature ($T_e = 15$ eV) and the neutral density n_0: $\nu = n_0 < \sigma v >$. The neutral density should be $n_0 = 4\times10^{18}$ m^{-3} to allow an axial electron velocity $v_z = 700\, m.s^{-1}$. For a $5\, mg.s^{-1}$ flow rate and for the gas temperature of 800 K measured in the channel [4], the averaged neutral density in the near anode zone is $n_{0Max} = 5\times10^{19}$ m^{-3}. The above data are fully consistent with an electron transport induced by electron-neutral collisions. These data have been obtained for a T_{OFF} value of 10 µs; a neutral filling significantly higher than in the stationary regime is achieved near the channel output when the switch is turned leading to a neutral concentration higher than expected in the stationary regime [23]. Another conclusion is that the ionisation wave velocity is significantly higher than the average axial neutral velocity, which is in the range of 300 m/s. The possible impact of this difference on the CEDT's behaviour is considered below.

III.2.2. Comparison of transient behaviour of SPT and ATON thrusters.

An other CEDT has been studied. This thruster, known as the ATON thruster was developed at MIREA , Moscow [24] and a slightly modified version of such a thruster has been developed by SNECMA [25]. These structures differ from the SPT one by a different magnetic topography, the channel geometry being very close. The most attractive properties of the ATON structure are their ability to have optimised working operation with an extremely stable current regime, high efficiency and low plume divergence.

The space resolved OF diagnostic is not available on this structure but the switch experiments have been done on this thruster for comparison of the thruster current behaviour with SPT data. Comparative data are shown on Figure 19:. The first evidence is the much stronger stability of ATON CEDT: the permanent regime is restored within one single oscillation. The second evidence is the longer pseudo-period of the current transient.

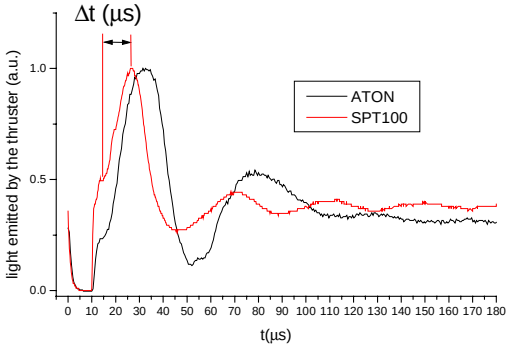

Figure 19: SPT and ATON thrusters response to a T_{OFF}=10µs discharge extinction.

These two characteristics seem to be related to the relative value of the axial neutral velocity and the ionisation wave velocity. This last characteristic cannot be measured on ATON CEDT, due to the lack of optical fiber data. It has been deduced from the comparison of the time ΔT required to achieve the first maximum of the current signal. The Figure 20 shows the variation of ΔT for SPT and ATON structures as function of T_{OFF}. These data have been obtained for the same neutral density, the same discharge voltage and almost the same channel geometry. For a given value of T_{OFF}, the neutral front displacement is similar for the two thrusters and these data can be interpreted in terms of ionisation wave velocity. The result, as indicated on the figure, is that this velocity is much closer of the neutral axial velocity for the ATON structure. It is clear that such a system should be much more stable against natural of driven perturbations, as evidenced on Figure 19:.

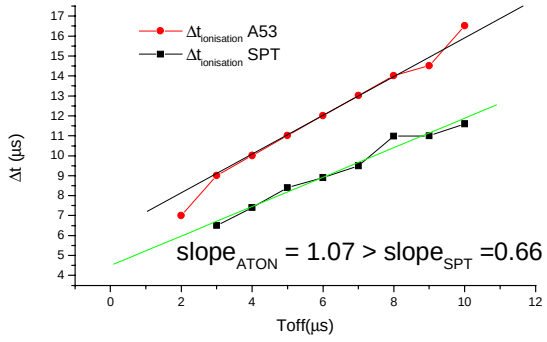

Figure 20: Variation of ΔT for SPT and ATON structures as function of T_{OFF}

III 2 3 : Cathode and anode currents waveforms

The switch is installed on the anode line of electrical of the thruster cable and the hollow cathode is connected both to the discharge current return line

and the heating power supply. The waveforms of currents on the discharge lines have been recorded simultaneously by using two identical, wide band, Tektronix probes. The Figure 21 shows the currents measured with a switch T_{OFF} of 10 µs.
The first interesting conclusion is that the initial rise of currents at 10 µs are similar. It means that the input of electrons driving the ionisation wave in the channel described before corresponds well to electrons coming from the cathode.
The second conclusion is that a delay is clearly observed between the maximum of anode current and the maximum of cathode current. This delay has a straightforward explanation. Its value is 4 µs. The time required for the ion beam front to reach the region where the magnetic field is low enough for a free access for neutralising electrons can be estimated. With an ion velocity of the order of 20.000 m/s and a distance of 5-10 cm this time is 2.5-5 µs. The burst of cathodic current is due to the electron flow required for neutralisation of the ion burst. It means that a reasonable explanation is that the cathodic current burst is connected to the ion burst neutralisation.

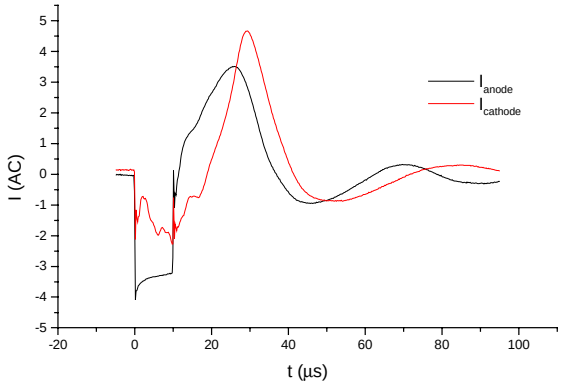

Figure 21: Cathode and anode current waveform.

III.3: evidence of electron drift micro-instabilities connected to discharge current transients

The last and original result obtained in these studies of transient behaviour concerns the observation of microinstabilities and their relation with SPT100 current waveform.
The probe of electron drift current has a wide band response, as shown by data obtained in the switch experiments. Single shot probe and thruster current signals have been recorded by using a two channels fast sampling scope at a rate of 1 GHz and with 10.000 sample per run. The probe signal has been processed by using a gliding Fourier transform procedure and a typical result of such experiment is shown on Figure 22.

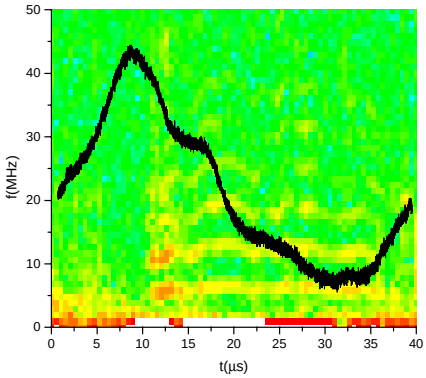

Figure 22:Discharge current and gliding Fourier transform of the inductive loop signal (single shot).

It appears clearly that a well-localised instability is observed, with fundamental frequency varying in the range 7-8 MHz and its harmonics till the 5^{th} are also observed. The location in time is clearly related to the discharge current behaviour. When the instability arises, the slope of the current shows a transition towards higher current values. To our knowledge this is the first evidence of correlation between microinstability and macroscopic transport phenomena. The statistical existence of such phenomena is evidenced by recording the same signals but in the averaged mode of the sampling scope acquisitions (average on 128 successive runs). The result, as shown on Figure 23, is connected to statistically independent events, taken at various instantaneous states of the discharge current. The only common property is of the superposed runs is that the triggering of these runs is achieved for a given current fluctuation level. As can be seen the localisation of the instability is more smoothly distributed in time for this averaged experiment, as well as the perturbation of the current waveform. Nevertheless the same property remains evidenced near the triggering time: these instabilities appear in the decreasing period of the discharge current.
The frequency of this instability is of the order of the natural frequency of rotation of electrons in the magnetised zone of the channel. For the estimated values of the electric field ($3\ 10^4$ V/m), of the radial magnetic field (150 G) and of electron loop length (27 cm) this rotation frequency should be of the order of 7 MHz. These instabilities have been predicted analytically with a collisionless treatment and also reported experimentally by Esipchuck and Tilinin [26]. 2D stability analysis taking into account the collisional nature of the plasma also seems to evidence unstable modes in the MHz

frequency range ([27], [28]). However no data exist concerning microinstabilities correlation with the thruster current.
2D, full PIC, simulations developed in France, at Ecole Polytechnique [29], leads to their evidence and, moreover suggest that they can be involved in an enhanced axial electron transport. This simulation is in progress and the present experimental data reinforce their interest, as they support, for the first time, the idea of such enhanced electron transport.

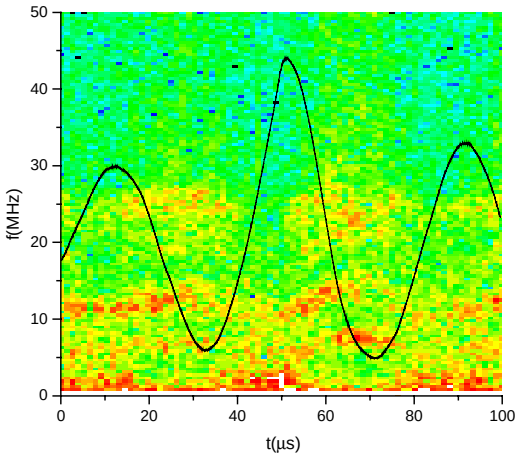

Figure 23: Discharge current and gliding Fourier transform of the inductive loop signal (average 128 triggered on I_d)

Conclusion

The development of a co-operative research program was launched few years ago in France in order to improve the knowledge on the physics of closed electron drift thrusters. The program includes both experimental and simulation/modelling studies. This paper is focused on a new experimental approach of the physics of these thrusters by using very fast and short interruptions of the thruster current. This approach was shown to be a very instructive one in many aspects.
A wide frequency band electromagnetic probe has been used for the measurement of the electron drift current. This current is shown to be of 20-25 A for a discharge current of 4.3 A. Probe data show that fast current interruptions (< 0.2 µs) induce also very fast cancellations of the electric field in the channel.
Detailed space resolved spectroscopic transient data have been used to derive some insights on the electron population in the active zone of the channel. The analysis of the behaviour of neutral and ionic levels shows that metastable states play a significant role and should be included in modelling, especially for the creation of double charged ions.
Time of flight phenomena can be used to derive in a simple way the features of the plume in terms of contributions of single and multiple charge ions. Double charged ions are shown to be created in the channel at a potential close to but lower than the potential where single charge ions are created and their angular distribution is consequently different from the distribution of single charge ions in the plume.
Measurements of the axial electron velocity in the active channel zone have been derived from space and time resolved optical data. This velocity is in the range of the value derived from electron-neutrals collisions taking into account electron-neutral collisions. The comparison of two thrusters shows that this velocity is involved in the unstable behaviour of closed electron drift thrusters.
Finally, for the first time, a correlation between microinstabilities and transport processes has been evidenced. This instability is characterised a fundamental frequency of 6-9 MHz, with harmonics up to the 5^{th} , and is clearly related to the electron azimuthal drift. Its development is localised in time: bursts of instability signals are observed during thruster current fluctuations and have an impact on the current waveform.
Besides the experimental work described in this paper the French research program includes modelling/simulation studies through hybrid or pure PIC codes. For both, the development of 2D codes is in progress and the above instabilities and their impact on axial electron transport are revealed also by preliminary data of 2D PIC codes.

This program is developed in the frame of a co-operative structure (GDR N°2232) involving CNES-SNECMA-ONERA and academic CNRS-University laboratories. The next step in this program will concern an up-scaled and improved version of closed electron drift thruster, with a power in the range 6 kW.

Bibilography

[1] Morozov A.I. et al., Zh. Tekh. Fiz. **42**, 612 (1972). [Sov. Phys. Tech. Phys. 17, 482 (1972)].
[2] Janes G.S. and Lowder R.S., Phys. Fluids **9**, 1115 (1966).
[3] Cadiou A., Gelas C., Darnon F., Jolivet L., Pillet N., "An Overview of th CNES Electric Propulsion Program",

27th International Electric Propulsion Conference, Passadena, October 2001.

[4] Touzeau M.; Prioul M.; Roche S.; Gascon N.; Perot C.; Darnon F.; Bechu S.; Philippe-Kadlec C.; Magne L.; Lasgorceix P.; Pagnon D.; Bouchoule A.; Dudeck M., "Plasma diagnostic systems for Hall-effect plasma thrusters", Plasma Physics and Controlled Fusion, Dec. 2000; **42** Suppl. 12B : B323-B339.

[5] Bouchoule A.; Philippe-Kadlec C.; Prioul M.; Darnon F.; Lyszyk M.; Magne L.; Pagnon D.; Roche S.; Touzeau M.; Bechu S.; Lasgorceix P.; Sadeghi N.; Dorval N.; Marque J.P.; Bonnet J., "Transient phenomena in closed electron drift plasma thrusters: insights obtained in a French cooperative program", Plasma Sources Science and Technology, may 2001; 10 (2) : 364-377.

[6] Philippe-Kadlec C., Laure C., Bouchoule A., 33th AIAA/ASME/SAE/ASEE Joint Propulsion Conference and Exhibit, Seatle (1997).

[7] Darnon F., Philippe-Kadlec C., Bouchoule A., Lyszyk M., "Dynamic Plasma and Plume Behavior of SPT Thrusters", AIAA 98-3644, 34th AIAA/ASME/SAE/ASEE Joint Propulsion Conference and Exhibit, Cleveland (1998).

[8] Roche S., Gascon N., Prioul M., Magne L., Bechu S., Bouchoule A., Lasgorceix P., Pagnon D., Perot C., Albarède L., Touzeau M., Dudeck M., Lyszyk M., " Operating Conditions and Plasma Study of an ATON-Class Hall Thruster", 3rd Spacecraft Propulsion Conference, Cannes (2000).

[9] Béchu S., Gascon N., Roche S., Prioul M., Albarede L., Lasgorceix P., Dudeck M., "Comparison between two kinds of Hall Thrusters: SPT100 AND ATON", AIAA 00-3524, 36th AIAA/ASME/SAE/ASEE Joint Propulsion Conference and Exhibit, Huntsville (2000).

[10] Prioul M. , Roche S. , Pagnon D., Magne L., Touzeau M., Bouchoule A., Lasgorceix P., "Insight on Closed Electron Drift Thrusters obtained with a Discharge Shutter as Diagnostic Tool", AIAA-2001-3358, 37th AIAA/ASME/SAE/ASEE Joint Propulsion Conference and Exhibit, Salt Lake City (200).

[11] Darnon F., Phd Thesis, Orléans University (1999).

[12] Lasgorceix P. *et al.*, Proc. 20th Symposium in Rarefied Gas Dynamics, Beijing (1996).

[13] Morozov A.I. and Savelyev V.V. "Fundamentals of Stationnary Plasma Thruster Theory", Reviews of Plasma Physics n° 21 edited by Kadomtsev B.B. and Shafranov V.D.,ISBN 0-306-11064-4, Plenum Publisher, New York, (2000).

[14] Haas J.M. and Gallimore A.D., "Consideration on the Role of the Hall Current in a Laboratory-Model Thruster", AIAA-2001-3507, 37th AIAA/ASME/SAE/ASEE Joint Propulsion Conference and Exhibit, Salt Lake City (2001).

[15] Dorval N., Bonnet J., Marque J.P., Chable S., Rogier F., Lasgorceix P., Rosencher E., "Determination of the ionization and acceleration zones in a Stationary Plasma Thruster by optical spectroscopy study: experiments and model", Journal of Applied Physics (submitted).

[16] Garrigues L.; Heron A.; Adam J.C.; Bœuf J.P.,"Hybrid and particle-in-cell models of a stationary plasma thruster", : Plasma Sources Science and Technology, **9** (2) : 219-226 (2000).

[17] Prioul M., Irzyk M., Laure C., Bouchoule A., "Time of flight ion beam analyzer : a small-scale design and applications", ISPC 2001, Orléans (200)1.

[18] Philippe-Kadlec C., Phd thesis, Orléans University (1998).

[19] Perot C., Gascon N., Lasgorceix P., Hauser A., Dudeck M., 35th AIAA/ASME/SAE/ASEE Joint Propulsion Conference and Exhibit, Los Angeles (1999).

[20] Sadeghi N. et al., internal report NT 98-3, Laboratory LSP Grenoble.

[21] Griffin D.C., Bottcher C., Pindzola M.S., Younger S.M., Gregory D.C. Crandall D.H., "Electron-impact ionzation in the xenon isonuclear sequence" Phys. Rev. A., vol 29, n° 29 (1984).

[22] Gascon N. Phd Thesis, Marseille University, 2000.

[23] Bœuf J.P., Garrigues L., "Low frequency oscillations in a stationary plasma thruster", J. Appl. Phys. **84** (7), 3541 (1998).

[24] Morozov A.I.,Bugrova A.I., Desyatshov A.V., Ermakov Yu. A., Kozintseva M.V., Lipatov A.S., Pushkin A.A., Khartchevnikov V.K., and Churbanov D.V., "ATON-Thruster Plasma Accelerator", Plasma Physics Reports, vol. 23, no. 7, 1997.

[25] Bugeat J.P., Koppel C., "Development of a second generation of SPT", International Electric Propulsion Conference, Moscow, 1995, IEPC-95-35

[26] Esipchuk Y.V., Tilinin G.N., "Drift instability in a Hall-current plasma accelerator", Zh. Tekh. Fiz **46** 718-729 (1976) [Sov. Phys. Tech. Phys. **21**, 417 (1976).

[27] Chesta E., Meezan N.B., Cappelli M.A.,"Stability of a magnetised Hall Plasma Discharge", J. Appl. Phys. **89** n°6 3099 (2001).

[28] Choueri E.Y., "Plasma oscillations in Hall thrusters", Phys. Plasma **8** n°4 1411 (2001).

[29] Heron A., Adam J.C., internal report DTS/AE/MTE/3P-01 235 (2001).